

Oscillatory behaviour in a three-component plankton population model

Andrew M. Edwards and John Brindley

*Department of Applied Mathematical Studies and Centre for Nonlinear Studies,
University of Leeds, Leeds LS2 9JT, UK*

(Received March 1996; final version August 1996)

Abstract. *We examine the qualitative behaviour of an NPZ (nutrient–phytoplankton–zooplankton) model for parameter ranges consistent with values used in the literature. The wide range of values partly reflects variations of conditions in different environments for the plankton, but in many cases is a measure of the difficulties in making observations and consequent uncertainties. We pay particular attention to the bifurcational behaviour of the system, and to the regions of parameter space for which oscillatory behaviour is possible; such oscillatory behaviour has recently been found in both observational data and in more complex ecosystem models. In some regions of parameter space, we also find that multiple attractors occur. Finally, we examine in more detail the behaviour for a range of values of nutrient input.*

1 Introduction

Plankton play a key role in ocean–atmosphere dynamics. Their effects range from alterations on a local scale of the sea surface temperature and mixed layer depths, to ocean-basin-wide emissions of potentially important climatological gases such as dimethyl sulphate, and to global fluxes of atmospheric carbon. These effects occur over a wide range of spatio-temporal scales and via a number of different biophysical processes. Phytoplankton and zooplankton also form the basis of marine food webs throughout the world’s oceans, supporting a diverse range of marine and terrestrial life from shrimps and cod to blue whales and man. Thus, understanding the dynamics of plankton populations is of major importance in predicting future fish harvests and in assessing the possible consequences of global warming.

Direct measurement of the biomass comprised by plankton, either of the plant-like, photosynthesizing phytoplankton, or of the myriad species of herbivorous zooplankton, is difficult and expensive. Historically, data has come

Table 1. Abbreviations, default values and ranges of the parameters. The ranges are those used by a variety of authors in different models, and are discussed in Section 3

Parameter	Symbol	Default value	Reported range
<i>a/b</i> gives maximum <i>P</i> growth rate	<i>a</i>	0.2 m ⁻¹ day ⁻¹	0.1–0.6
Light attenuation by water	<i>b</i>	0.2 m ⁻¹	0.04–0.2
<i>P</i> self-shading coefficient	<i>c</i>	0.4 m ² g ⁻¹	0.3–1.2
Higher predation on <i>Z</i>	<i>d</i>	1 m ³ g ⁻¹ day ⁻¹	0.25–2.0
Half-saturation constant for <i>N</i> uptake	<i>e</i>	0.03 g m ⁻³	0.02–0.15
Cross thermocline exchange rate	<i>k</i>	0.05 day ⁻¹	0.0008–0.13
<i>P</i> respiration rate	<i>r</i>	0.15 day ⁻¹	0.05–0.15
<i>P</i> sinking loss rate	<i>s</i>	0.04 day ⁻¹	0.032–0.08
<i>N</i> concentration below mixed layer	<i>N</i> ₀	0.6 g m ⁻³	0.1–2.0
<i>Z</i> assimilation efficiency	α	0.25	0.2–0.75
<i>Z</i> excretion fraction	β	0.33	0.25–0.8
Regeneration of <i>Z</i> predation excretion	γ	0.5	0.5–0.9
Maximum <i>Z</i> grazing rate	λ	0.6 day ⁻¹	0.6–1.4
<i>Z</i> grazing half-saturation coefficient	μ	0.035 g m ⁻³	0.02–0.1

from analyses of samples taken 'over the side' from ships; it is inevitably sparse and patchy. More recently, it has been possible to use satellite observations, though the identification and interpretation of that part of the radiation spectrum which relates to plankton is a formidable task.

In this situation, theoretical modelling of plankton population dynamics is an essential requisite for our understanding of the physical processes which affect the dynamics, and of the consequences for the oceans and atmospheric environment of changes in those dynamics. For example, large changes either in total biomass or its distribution in space and time could have major, perhaps catastrophic, consequences for human food supply, either directly, through fish population decline, or indirectly through adverse climate change.

The extensive literature devoted to the mathematical modelling of plankton populations may be divided crudely into the class of complex, compartmental models, which seek to contain a faithful representation of the physics and/or the biology, and are, therefore, from a mathematical viewpoint too complex for theoretical analyses (e.g. Fasham *et al.*, 1990; Sarmiento *et al.*, 1993), and the class of simple 'caricature' models, which seek rather to expose crucial qualitative features and their relationship to or dependence on physical processes (e.g. Evans & Parslow, 1985; Steele & Henderson, 1981; Truscott & Brindley, 1994).

The first class, usually consisting of many coupled nonlinear differential equations, is amenable only to numerical experimentation; uncertainties in the values of many parameters often frustrate accurate agreement with observation, but diagnostic analysis of the dynamics of the numerical experiments should throw light on crucial physical features and controls. The second class, of which this paper is an example, recognizes the uncertainties and shortcomings in observational data, and instead seeks to explore simple dynamical models in order to recognize and classify the range of possible qualitative behaviour to be expected from the system. These uncertainties are reflected in the range of values which have been used by recent authors for parameters measuring important effects. They are given in Table 1, and form the basis for our own range of parameter values for investigation.

Ryabchenko *et al.* (1996) have recently investigated the occurrence of short-term oscillations which can arise in both phytoplankton data (Williams, 1988) and in the

output of large ecosystem models (Fasham, 1993; Fasham *et al.*, 1993). Such oscillations occur some years in the North Atlantic Ocean during the summer, and have a period of the order of 1 month. For the remainder of the year, such short-term oscillations do not occur. This suggests that the seasonal forcing of some of the parameters may be taking the system from a region of parameter space where the unforced system would be attracted to a stable steady state, into a region during the summer months where the unforced system would exhibit stable oscillatory behaviour. We demonstrate the existence of such a region of oscillatory behaviour for a three-component plankton model, and illustrate how this region persists as each of the parameters in the model are varied.

Our approach is to model the evolution of phytoplankton (P) whose growth is driven, plant-like, by photosynthesis, and herbivorous zooplankton (Z) which graze on the phytoplankton. Essential nutrient (N) is regarded as a third, potentially growth-limiting variable in an NPZ model. The gross lumping of all phytoplankton together in a single population, regardless of species or age, and the same with zooplankton, clearly deprives the model of any realistic quantitative potential, but nevertheless retains the essential differences in function which determine broad qualitative features.

The choice of functional form for zooplankton mortality is biologically controversial and potentially influential on the qualitative dynamics of the system. Steele and Henderson (1992) investigated a similar NPZ model to ours; in contrast to their findings that, for their particular parameter values, limit cycle behaviour which occurs for linear zooplankton mortality does not occur when quadratic zooplankton mortality is used, our model, which has quadratic zooplankton mortality, exhibits limit cycle behaviour over a broad parameter range.

The mathematical model is presented in Section 2, with a discussion of the functional forms used, together with the parameter ranges which have been extracted from other models, given in Section 3. A brief analysis is presented in Section 4, and Section 5 contains the main numerical results, illustrating the persistence of oscillatory behaviour. These are summarized and discussed in Section 6.

2 The mathematical model

We follow closely the approach of Steele and Henderson (1981), hereafter referred to as SH81, using a simple three-compartment model explicitly representing nutrient, phytoplankton and herbivores, the concentrations of which are given by N , P and Z respectively. The interactions between these components are illustrated in Fig. 1, and are explained below. We assume that the layer in which the plankton growth takes place is thoroughly mixed at all times, so that there are no spatial gradients of concentrations and the changes in N , P , Z can be represented by three coupled ordinary differential equations:

$$\frac{dN}{dt} = -\text{uptake} + \text{respiration} + Z \text{ excretion} + Z \text{ predation excretion} + \text{mixing}$$

$$\frac{dP}{dt} = \text{uptake} - \text{respiration} - \text{grazing by } Z - \text{sinking} - \text{mixing}$$

$$\frac{dZ}{dt} = \text{growth} - \text{higher predation}$$

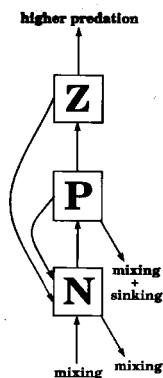


Fig. 1. Interactions between nutrients (N), phytoplankton (P) and zooplankton (Z), plus input to and losses from the system.

The specific functional forms used (discussed in Section 3) are:

$$\frac{dN}{dt} = -\frac{N}{e+N} \frac{a}{b+cP} P + rP + \frac{\beta\lambda P^2}{\mu^2 + P^2} Z + \gamma dZ^2 + k(N_0 - N) \quad (1)$$

$$\frac{dP}{dt} = \frac{N}{e+N} \frac{a}{b+cP} P - rP - \frac{\lambda P^2}{\mu^2 + P^2} Z - (s+k)P \quad (2)$$

$$\frac{dZ}{dt} = \frac{\alpha\lambda P^2}{\mu^2 + P^2} Z - dZ^2 \quad (3)$$

Units of N , P and Z are g C m^{-3} , and time units are days. The conversion equivalences, as used by SH81, are $1 \text{ g C} \equiv 20 \text{ mg Chl} \equiv 10 \text{ mg at N}$, where C is carbon, Chl is chlorophyll and N here is nitrogen. All parameters are positive, with $\alpha + \beta \leq 1$ and $\gamma \leq 1$ required from their definitions, and $r + s + k < a/b$, so that the phytoplankton do not die out when nutrient is infinitely abundant. The original SH81 model considered mesocosm experiments (mesocosms are giant plastic test-tubes, 5–10 m in diameter and 15–20 m deep, which are placed in the sea, enclosing a fixed volume of sea water). We have adapted it to the more usual 'open sea' case by incorporating diffusive mixing with deep water, in a similar fashion to Steele and Henderson (1993), but we have not yet considered a varying mixed layer depth. The only difference between our model and that of SH81 is, therefore, the inclusion of the $-kN$ term in (1) and the $-kP$ term in (2). We discuss the value of k , related to the mixed layer depth, in Section 3.

The equations have not been non-dimensionalized. Although this is not usual mathematical practice, it means that, when a parameter is varied in the model, it is clear exactly which single biological or physical effect is being considered. In fact, non-dimensionalizing the system only reduces the number of parameters from 14 to 9, which is not worthwhile for the analysis. Also, a , b and c could be redefined as two distinct parameters, but are kept separate as b represents a physical property of the water, while c is the self-shading effect of the phytoplankton, and a/b gives

the maximum phytoplankton growth rate, all of which have different values in different models.

3 The range of parameter values

Table 1 gives our default parameter values, taken from SH81, plus the range of values used by many authors; these partly reflect different geographical or other physical influences, but are largely attributable to uncertainties and lack of data.

The models considered, which are of both types mentioned in the introduction, are abbreviated as follows: Steele and Frost (1977)—SF77; Evans and Parslow (1985)—EP85; Frost (1987)—Fr87; Hofmann and Ambler (1988)—HA88; Wroblewski (1989)—Wr89; Fasham *et al.* (1990)—FDM90; Taylor and Joint (1990)—TJ90; Steele and Henderson (1992)—SH92; Fasham (1993)—Fa93; Steele and Henderson (1993)—SH93; Armstrong (1994)—Ar94; and Henderson and Steele (1995)—HS95.

A description of the functional forms we use (in the order in which they appear in the equations) and the parameter ranges used by other authors (converted into g C m^{-3} values using the aforementioned equivalences) are given below. Variation of parameter values across models is inevitable and direct comparisons are not always easy since different functional forms are sometimes used, but in many cases the parameter definitions are the same, allowing Table 1 to be constructed.

Following SH81, we consider a fixed mixed layer depth of 12.5 m. This choice of fixed depth is borne out by the data given by FDM90, Fa93 and SH93 at Bermuda Station "S" and Ocean Weather Station "India" in the North Atlantic Ocean, which display remarkable uniformity of mixed layer depth over the period May–October. The mixed layer deepens considerably during the winter months and inclusion of this process explicitly into the model would require a forcing (time-dependent) function, plus incorporation of a dilution rate of the N , P and Z concentrations (see EP85). However, it is insightful to first understand the behaviour of the unforced system. The mixed layer depth is implicitly incorporated in the values of a , k and s , as is discussed below.

A Michaelis–Menten function $N/(e+N)$ models nutrient uptake by phytoplankton; a standard choice by many authors. Values of the half-saturation constant e vary from 0.02 (g m^{-3}) by Wr89 and SH93, to 0.03 by SH81 (thus our default value is 0.03), 0.05 by EP85 and FDM90, 0.1 by Fr87 and 0.15 by HA88.

The term $a/(b+cP)$ represents (non-nutrient-limited) phytoplankton growth with limitations due to both light attenuation by the water (b) and self-shading of the phytoplankton (c). This term was equated by SH81 to the depth-averaged daily phytoplankton growth rate $2.58 P_{\max}/(b+cP)M$ derived by SF77, where P_{\max} is the maximum phytoplankton growth rate under optimal light conditions and M represents the depth of the mixed layer. Thus, a is defined by $a=2.58 P_{\max}/M$, where M takes the fixed value of 12.5 m, and a/b gives the maximum growth rate averaged over the depth of the mixed layer.

The rate P_{\max} has been assumed to take a broad range of values; 0.5 (day^{-1}) by HS95, 1.25 for Ocean Weather Station "India" and 2.9 for Bermuda Station "S" in Fa93, and 2.0 by EP85 and Wr89, resulting in a range for a of 0.1–0.6 ($\text{m}^{-1} \text{day}^{-1}$), the default value being $a=0.2$. Ar94 did not consider self-shading, but had an equivalent a/b rate of 0.7 for a micronutrient-limited case and 1.4 for a standard case which, using our default value of $b=0.2$, falls within the range just discussed.

Light attenuation by the water is represented by b , where $b=(\ln 100)/z_e$

corresponds to the 1% light maximum at a depth of z_e m (taken by SH81 to be 20 m, giving $b=0.2 \text{ m}^{-1}$). SF77, EP85 and HS95 used $b=0.1 \text{ (m}^{-1}\text{)}$, corresponding to $z_e=46$ m, the usual definition for the euphotic zone, while Fa93 and SH93 took $b=0.04$, giving $z_e=115$ m. The term cP represents phytoplankton self-shading; as the phytoplankton concentration increases, the average light received per organism, and therefore the average growth rate, is reduced. The coefficient c , for which SH81 used the SF77 value of $0.2^+ (\text{g m}^{-3})^{-1} \text{ m}^{-1}$, was taken to be 0.3 by SH93 and Fa93, 0.5 by HS95, and EP85 used 1.2, while suggesting the possible use of 0.6.

The default respiration rate of $r=0.15 \text{ (day}^{-1}\text{)}$ from SH81 is the SF77 value at 10°C for a $10\text{-}\mu\text{m}$ diameter cell at the North Sea temperature. HS95 used 0.05 and EP85 used 0.07. FDM90 had no respiration term as such, but they did have an equivalent natural mortality rate of 0.09 day^{-1} , some of which is subsequently recycled back through the microbial loop, becoming a food source for both phytoplankton and zooplankton. FDM90 found that this linear phytoplankton loss was the most sensitive and hardest to measure parameter, and allowed it to vary freely in order to fit the data. Our respiration term is recycled immediately into nutrient (as were those of HS95 and EP85), while none of our linear sinking term is recycled.

A sigmoidal Holling type III zooplankton grazing term, $\lambda P^2/(\mu^2 + P^2)$, is used, with maximum zooplankton grazing rate of $\lambda=0.6 \text{ (day}^{-1}\text{)}$ and half-saturation constant of $\mu=0.035 \text{ (g m}^{-3}\text{)}$. The type III form is chosen by SH81 (and SH93) based on the zooplankton grazing data presented by Adams and Steele (1966), which indicates low grazing rates at low phytoplankton concentrations. EP85 used a Holling type II (or Michaelis–Menten) function with a lower grazing threshold. Such a function can be smoothly approximated by the type III function with the same values of λ and μ , and can be inferred from the data of Parsons *et al.* (1969). HS95 used a type II function, the seven-component model of FDM90 had alternative food sources (phytoplankton, bacteria and detritus) for the zooplankton, while Ar94 used a non-standard piecewise linear function (for simplification reasons), but in all cases, equivalent values of λ and μ were given. The values used for λ were 1.0 by FDM90, SH93 and HS95, and 1.4 by Ar94, while μ was taken to be 0.02 by SH93, 0.025 by HS95, and 0.1 by EP85 and Ar94.

The zooplankton assimilation efficiency α varies widely—SH93 used 0.2, EP85 and SH92 used 0.5, while Fa93 used 0.75. The regeneration fraction β in SH92 and SH93 was such that $\alpha + \beta = 1$, and the remaining fraction $1 - \alpha$ in Fa93 was also recycled into the system. These correspond to respective values for β of 0.5, 0.8 and 0.25, while such regeneration was not considered by EP85. Our default values of $\alpha=0.25$ and $\beta=0.33$ sum to 0.57, allowing both regeneration and a loss from the system.

Higher predation of the zooplankton by invertebrate carnivores, such as ctenophores, is modelled as the quadratic form $-dZ^2$, as the carnivore population is assumed to change in proportion to the zooplankton population. SH81 showed, for their mesocosm case, the initial paths of some trajectories of the system for various values of d . They noted that the system changed its behaviour significantly at a value of d around $1.0 \text{ (g m}^{-3}\text{)}^{-1} \text{ day}^{-1}$; their range of d considered was 0.25–1.75. Their results, together with the fact that d is a particularly difficult parameter to measure and assign a fixed value to (SH93 stated that in any model it is essentially a free choice), motivate us to use d as the primary bifurcation parameter.

We have commented earlier on the potential significance of the functional form of the zooplankton mortality closure term. SH93 used the quadratic form with a default value of $d=1.0$ which was allowed to vary in order to fit the model to data, and TJ90 also used a quadratic closure term, defining it as zooplankton cannibalism. SH81 and SH92 discussed the use of using either a linear or a quadratic function—FDM90 used the simple linear term $-DZ$.

A later investigation will address the consequences of using alternative functions, including the Holling-type functions which saturate for large Z . Such forms have been used in the higher-order models of Fr87, HA88 and Fa93, but require estimation of an extra poorly known parameter (see SH92). However, in a recent paper, Fasham (1995) investigated a six-component ecosystem model which explicitly modelled carnivores grazing on herbivorous zooplankton using a Holling type III function. He concluded that, if the carnivores are then not to be explicitly modelled (as in our case), then a quadratic closure term (in the herbivorous zooplankton equation) is indeed an appropriate function to use.

γ is the proportion of the zooplankton loss that is regenerated as nutrient, taken by SH81 and SH92 to be 0.5, and by SH93 to be 0.8. FDM90 considered linear zooplankton losses due to both mortality and excretion, of which 89% was retained in the system (but would undergo further losses before being utilized by phytoplankton), and 90% of the loss in Fa93 was similarly recycled. Some models (e.g. Franks *et al.*, 1986) consider a totally conservative system from which nothing is lost, thus $\gamma=1.0$, whereas EP85 did not consider any such recycling.

The $k(N_0 - N)$ term models the exchange of nutrients with the water below the mixed layer, where the exchange rate k defines the fraction of the mixed layer which is exchanged daily with the deeper water due to diffusive processes, and N_0 is the sub-mixed-layer nutrient concentration.

SH92 used $k=0.033$ (day^{-1}) and 0.1 and found that 0.033 gave a steady state of the system (which, when the system was forced, simply tracked the forcing), but 0.1 (or a larger N_0 value) resulted in limit cycles. FDM90 used a cross thermocline mixing rate of 0.1 m day^{-1} which Fa93 later decreased to 0.01 m day^{-1} to give an improved fit to summer phytoplankton data. Dividing these rates by our mixed layer depth (and their approximate minimum depth) of 12.5 m to obtain the daily exchange rate yields the respective values of $k=0.008$ (day^{-1}) and 0.0008. EP85 used a much higher mixing rate of 3 m day^{-1} (which they noted was a particularly uncertain estimate), and from their graph of seasonally varying mixed layer depth a range for k of 0.038–0.13 can be abstracted, the lower values representing winter levels due to a deep mixed layer (whereas the aforementioned low values of 0.008 and 0.0008 were due to low mixing rates).

FDM90 suggested the N_0 range of 0.1–0.2 (g m^{-3}) and used N_0 as a free parameter tuned so that the output best fitted the data, because of the difficulty in assigning a constant value to it. HS95 used $N_0=0.3$, TJ90 used 0.6, and EP85 used 1.0, while Fr87 took a range of 0.7–2.0.

The final parameter to be discussed is the sinking rate, s , of phytoplankton out of the mixed layer. SH81 took $s=0.04$ (day^{-1}) to correspond to a sinking velocity of 0.5 m day^{-1} , the same velocity used by SH93. FDM90 did not have a sinking term, but did have a linear phytoplankton mortality rate, as discussed earlier with respect to the respiration term. HS95 assumed a range of $0.4\text{--}1.0 \text{ m day}^{-1}$, with a varying mixed layer depth used to determine the loss rate, which would equal 0.032–0.08 using our fixed mixed layer depth.

4 Analysis

The analysis of this section provides the groundwork for the numerical investigation presented in Section 5, and may be skimmed through without compromising the understanding of the main numerical results. The powerful reduced nullsurface technique used by McCann and Yodzis (1995), in their analysis of the three-species food chain proposed by Hastings and Powell (1991), cannot be used here. This is due to the more complicated formulation of our equations, which is in part due to the recycling effects which are present in the system.

The steady states of the system and their stability are now calculated. The analysis of a general NPZ system by Truscott and Brindley (1994) and Truscott (1994) can be partly followed and is extended for our model. The stability of a steady state is determined by the eigenvalues of the Jacobian matrix, which is given by

$$\mathbf{A} = \begin{bmatrix} \frac{a\alpha P^2}{(e+N)^2(b+cP)} - k & -\frac{abN}{(e+N)(b+cP)^2} + r + \frac{2\beta\lambda\mu^2 PZ}{(\mu^2 + P^2)^2} & \frac{\beta\lambda P^2}{\mu^2 + P^2} + 2\gamma dZ \\ \frac{aeP}{(e+N)^2(b+cP)} & \frac{abN}{(e+N)(b+cP)^2} - r - s - k - \frac{2\lambda\mu^2 PZ}{(\mu^2 + P^2)^2} & -\frac{\lambda P^2}{\mu^2 + P^2} \\ 0 & \frac{2\alpha\lambda\mu^2 PZ}{(\mu^2 + P^2)^2} & \frac{\alpha\lambda P^2}{\mu^2 + P^2} - 2dZ \end{bmatrix}$$

evaluated at the steady-state values of N , P and Z .

There is a steady-state solution of the form $(N, P, Z) = (N_0, 0, 0)$, which exists for all parameter values. The Jacobian at $(N_0, 0, 0)$ is

$$\mathbf{A} = \begin{bmatrix} -k & -\frac{aN_0}{b(e+N_0)} + r & 0 \\ 0 & \frac{aN_0}{b(e+N_0)} - r - s - k & 0 \\ 0 & 0 & 0 \end{bmatrix}$$

It can be seen that there is always one zero eigenvalue for $(N_0, 0, 0)$ and the other two eigenvalues are $-k$ and Φ , where

$$\Phi = \frac{aN_0}{b(e+N_0)} - r - s - k$$

Truscott calculated the centre manifold for such a steady state, and concluded that, for $\Phi < 0$ $(N_0, 0, 0)$ is stable, and for $\Phi > 0$ it is unstable. At $\Phi = 0$, $(N_0, 0, 0)$ has two zero eigenvalues and undergoes a 'three-way transcritical bifurcation' of codimension two, which is discussed below. For the default parameter values $\Phi = 0.71$, and Φ remains positive as any one parameter varies over its reported range. Φ can become negative if more than one parameter is allowed to vary (but this only occurs for certain extreme values within the ranges), and thus Φ remains positive in our numerical analysis since we only vary one of these parameters at a time.

Two steady states of the form $(N_1^*, P_1^*, 0)$ and $(N_2^*, P_2^*, 0)$ also exist, where N_1^*, N_2^* are solutions to the quadratic equation

$$ckN^2 + \left[\frac{a(s+k)}{r+s+k} - b(s+k) + ck(e-N_0) \right] N - [b(s+k) + ckN_0]e = 0 \quad (4)$$

and P_1^*, P_2^* are given by

$$P_i^* = \frac{k(N_0 - N_i^*)}{s+k} \quad (5)$$

for $i = 1, 2$.

The discriminant of the quadratic is strictly positive, so the solutions for N_1^*, N_2^* are real and, furthermore, one is positive (call this N_1^*) while the other is always negative (N_2^*) since the constant term of the quadratic is negative. $(N_2^*, P_2^*, 0)$ can therefore never enter the positive octant. From (5), it is clear that $P_1^* > 0$ for $N_1^* < N_0$, and $P_1^* < 0$ for $N_1^* > N_0$. By considering the quadratic for P obtained by substituting (5) into (4) it can be shown that $P_1^* > 0$ for $\Phi > 0$ and $P_1^* < 0$ for $\Phi < 0$. When $\Phi = 0$, $(N_1^*, P_1^*, 0) = (N_0, 0, 0)$, which is the previously calculated steady state at the codimension-two bifurcation.

The third row of the Jacobian of $(N_1^*, P_1^*, 0)$ is

$$\left(0 \quad 0 \quad \frac{\alpha\lambda P_1^{*2}}{\mu^2 + P_1^{*2}} \right)$$

The third term is therefore an eigenvalue, and since it is always positive (for $P_1^* \neq 0$), the steady state $(N_1^*, P_1^*, 0)$ can never be stable.

From (3), it is clear that steady-state solutions (N^*, P^*, Z^*) with $Z \neq 0$ must satisfy

$$Z = \frac{\alpha\lambda P^2}{d(\mu^2 + P^2)} \quad (6)$$

Substituting this into (1) and (2), equating these equations to zero, and eliminating N from them, results in a tenth-order polynomial in P , the solution of which gives the non-zero steady-state value of P^* . Such a polynomial precludes the possibility of writing down an analytical form for (N^*, P^*, Z^*) . The constant term of the polynomial is Ψ , where

$$\Psi = bd^2k\mu^8(e + N_0)\Phi$$

Therefore, $\Psi \rightarrow 0$ as $\Phi \rightarrow 0$, and at $\Phi = 0$, $P = 0$ becomes a solution of the tenth-order polynomial. The (N^*, P^*, Z^*) solution thus degenerates to $(N_0, 0, 0)$, at the three-way transcritical bifurcation point $\Phi = 0$.

Equation (6) can be used to simplify the Jacobian at (N^*, P^*, Z^*) , which becomes

$$A = \begin{bmatrix} -\frac{aeP^p}{(e+N)^2(b+cP)} - k & -\frac{abN}{(e+N)(b+cP)^2} + r + \frac{2d^2\beta\mu^2Z^3}{\alpha^2\lambda P^3} & \left(\frac{\beta}{\alpha} + 2\gamma\right)dZ \\ \frac{aeP}{(e+N)^2(b+cP)} & \frac{abN}{(e+N)(b+cP)^2} - r - s - k - \frac{2d^2\mu^2Z^3}{\alpha^2\lambda P^3} & -\frac{dZ}{\alpha} \\ 0 & \frac{2d^2\mu^2Z^3}{\alpha\lambda P^3} & -dZ \end{bmatrix}$$

The third row of A now has two non-zero terms, and further analysis of the stability is not amenable. Hence, we now focus on the steady state (N^*, P^*, Z^*) for the numerical investigation of the system.

5 Numerical investigation

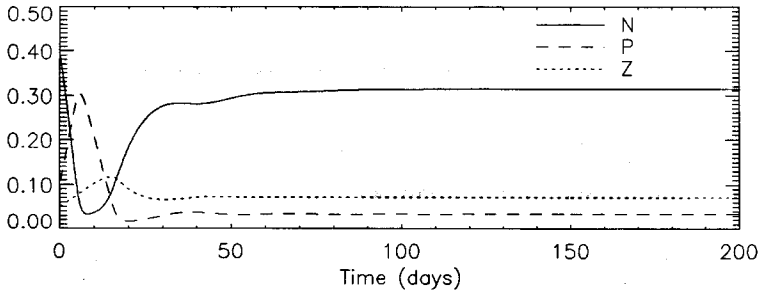
In this section, we investigate numerically how the dynamical behaviour of the system changes as parameters are varied. In Section 5.1, we present the trajectories of N , P and Z when all the parameters are set at their default values, and then show that this picture qualitatively changes when the higher predation on Z , d , is set at a higher value. Section 5.2 shows precisely how this bifurcation occurs by constructing one-parameter bifurcation diagrams for which d is continuously increased. Section 5.3 then indicates how these one-parameter diagrams will change as each of the other parameters in the model is varied, in turn, across the default ranges of values given in Table 1. This is done by tracking the location of Hopf bifurcations as each parameter is varied. In Section 5.4, we show explicitly how the one-parameter diagram for N changes as N_0 is increased, revealing an interesting array of dynamical behaviour.

The numerical analysis has involved a combination of the numerical bifurcation packages AUTO (Doedel *et al.*, 1994) and LOCBIF (Khibnik *et al.*, 1992) to examine the bifurcations, and the dynamical systems packages TraX (Levitin & Khibnik, 1991) and dstool (Guckenheimer *et al.*, 1991) to integrate and observe trajectories.

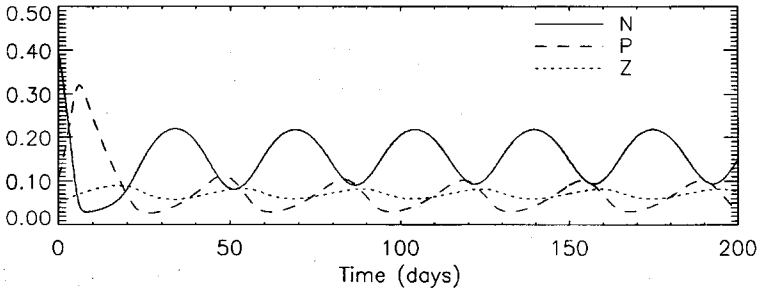
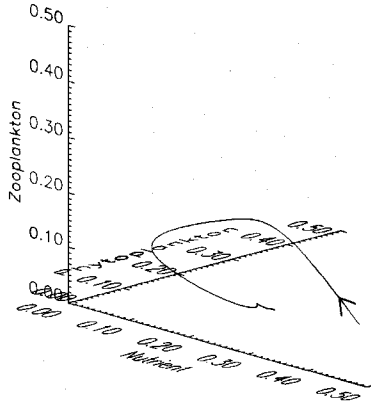
5.1 Time series and phase portraits

In Fig. 2(a), we show both the time series and the trajectory in N - P - Z space of the system from the initial condition $(N, P, Z) = (0.4, 0.1, 0.05)$, with all of the parameters fixed at their default values. It is seen that N , P and Z all settle down to steady-state values of $(N, P, Z) = (0.31, 0.034, 0.072)$ after a transient time of about 50 days. The initial large rise in P is due to the excitable nature of the system (see Truscott & Brindley, 1994), which can be deduced by plotting the two-dimensional nullsurfaces (which we do not show). Starting from a range of other initial conditions, trajectories converge to the same steady state, the transient time remains roughly the same and the actual nature of the transient trajectories depends upon the position of the initial points with respect to the nullsurfaces. By substituting the default parameters into equations (1), (2) and (3) and numerically solving the tenth-order polynomial discussed in Section 4, it can be shown that this steady state is the only steady state with strictly positive values of N , P and Z .

In Fig. 2(b), we increase the value of the higher predation on zooplankton, our primary bifurcation parameter d , from the default value of 1.0 to 1.5, and re-run the system from the same initial conditions. It is seen that the system now settles down to a periodic orbit, or limit cycle, after a short transient time. Again, this behaviour is independent of the initial conditions. The cycles show large amplitude fluctuations in N , but at values remaining lower than the steady-state value for $d=1.0$. The minimum cyclic value of P is roughly the same as the $d=1.0$ steady-state value, while Z undergoes small oscillations about the $d=1.0$ steady-state value. The oscillations have a period of 35 days, which is consistent with the aforementioned observational data and output of large ecosystem models.



(a)



(b)

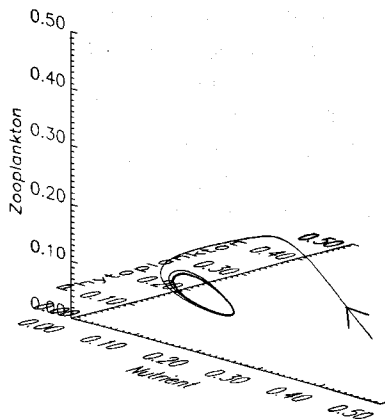


Fig. 2. The time series and phase space trajectory at two values of d , with all of the other parameters fixed at their default values. (a) $d=1.0$ — N , P and Z settle down to steady-state values after a short transient. (b) $d=1.5$ —the system settles down to a stable limit cycle.

5.2 One-parameter bifurcation behaviour

Clearly, there is a qualitative difference between Figs 2(a) and (b); the change from a steady state to oscillatory behaviour suggests that there has been a Hopf bifurcation at some value of d between 1.0 and 1.5. We now construct bifurcation diagrams in which d is varied continuously, indicating the exact value of d at which a Hopf bifurcation does indeed occur, and showing the steady-state values and limit cycle ranges of N , P and Z as d is varied.

Figure 3(a) shows how the steady-state value of the nutrient concentration, defined as N^* , varies as d changes, while the other parameters are kept fixed at their default values. At $d=1.0$, $N^*=0.31$, as indicated by Fig. 2(a). The solid line passing through $d=1.0$ in Fig. 3(a) indicates that the steady state is stable. As d increases from 1.0, the steady state goes from being stable (solid line) to unstable (dashed line) via a Hopf bifurcation (solid square) which is labelled A, and then regains stability at a second Hopf bifurcation, labelled B. At $d=1.5$, Fig. 2(b) showed that trajectories are attracted on to a stable limit cycle. This is indicated in Fig. 3(a) by the solid circles, which represent the maximum and minimum nutrient concentrations attained along the limit cycle.

Hopf bifurcation A is supercritical, which means that the branch of limit cycles which emanates from it is stable and coexists with the unstable steady state. Thus, in Fig. 3(a) the branch of limit cycles which emanate from Hopf bifurcation A appear as d is increased, rather than decreased. Hopf bifurcation B is also supercritical, so the resulting limit cycle branch appears as d is decreased, and it is seen that in fact just the one branch of limit cycles joins up the two Hopf bifurcations (i.e. no secondary bifurcations of the limit cycles occur).

Figures 3(b) and (c) are the equivalent diagrams for phytoplankton and zooplankton, which have default steady-state values of $P^*=0.034$ and $Z^*=0.072$. Although d is the predation rate on Z , the stable steady-state concentration Z^* (Fig. 3(c)) remains fairly constant for all except low d . A proportion γ (default value 0.5) of the higher predation is directly recycled into the system as the $+\gamma dZ^2$ term of the dN/dt equation (1), but increasing d actually causes the steady-state level N^* to decrease (Fig. 3(a)), due to the increase in P^* (Fig. 3(b)). Increasing predation on zooplankton would not directly cause the phytoplankton population to increase, and any definitive 'cause and effect' consequences cannot be deduced, due to the recycling effects propagating through the system.

During the oscillations, the value of P reaches levels far higher than those attained by any steady-state value, and for $d \in (1.48, 1.73)$ the maximum P value along the limit cycle is over three times the minimum value; the variations in the amplitude of Z are much smaller.

Figure 3(d) shows how the period of the limit cycles changes as d varies between the values at which the Hopf bifurcations occur (the only relevant range of d). It is clearly seen that the period is very insensitive to the value of d , remaining at the previously discussed value of 35 days across the whole range.

5.3 Two-parameter bifurcation behaviour

Figure 4 shows how the location of the two Hopf bifurcations changes as each of the other parameters is independently varied across the range reported in Table 1. The axis range plotted for each parameter is from 0 to (approximately) its maximum reported value. Figure 4 thus indicates how the steady-state bifurcation diagrams depicted in Fig. 3 will change as one other parameter is varied.

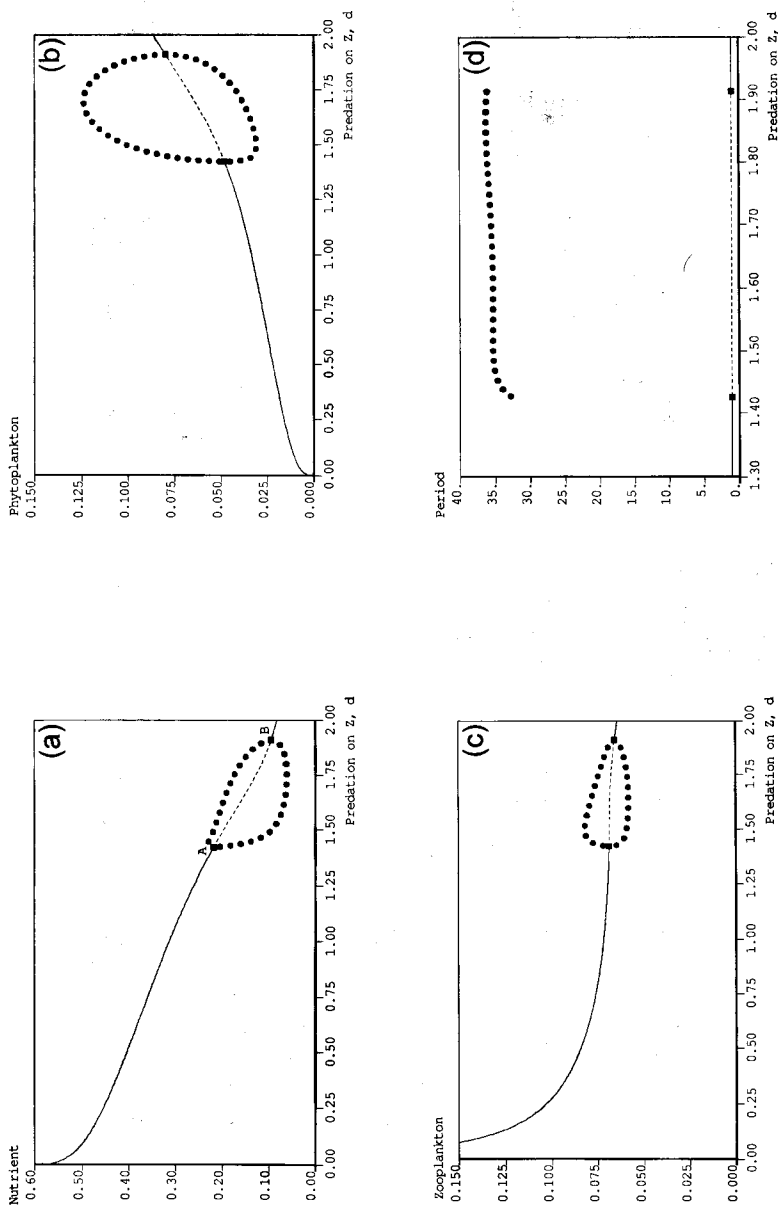


Fig. 3. Variations in the steady-state values of (a) nutrient, (b) phytoplankton and (c) zooplankton as d , the higher predation on the zooplankton, is changed. A solid line is a stable steady state, a dashed line is an unstable steady state, a solid square is a Hopf bifurcation and solid circles indicate the maximum and minimum values of the stable limit cycles. The Hopf bifurcations are labelled A and B to aid in later discussion. (d) The period of the limit cycles (solid circles) remains virtually constant throughout the region of oscillatory behaviour; the corresponding stability of the steady state is indicated by the horizontal line.

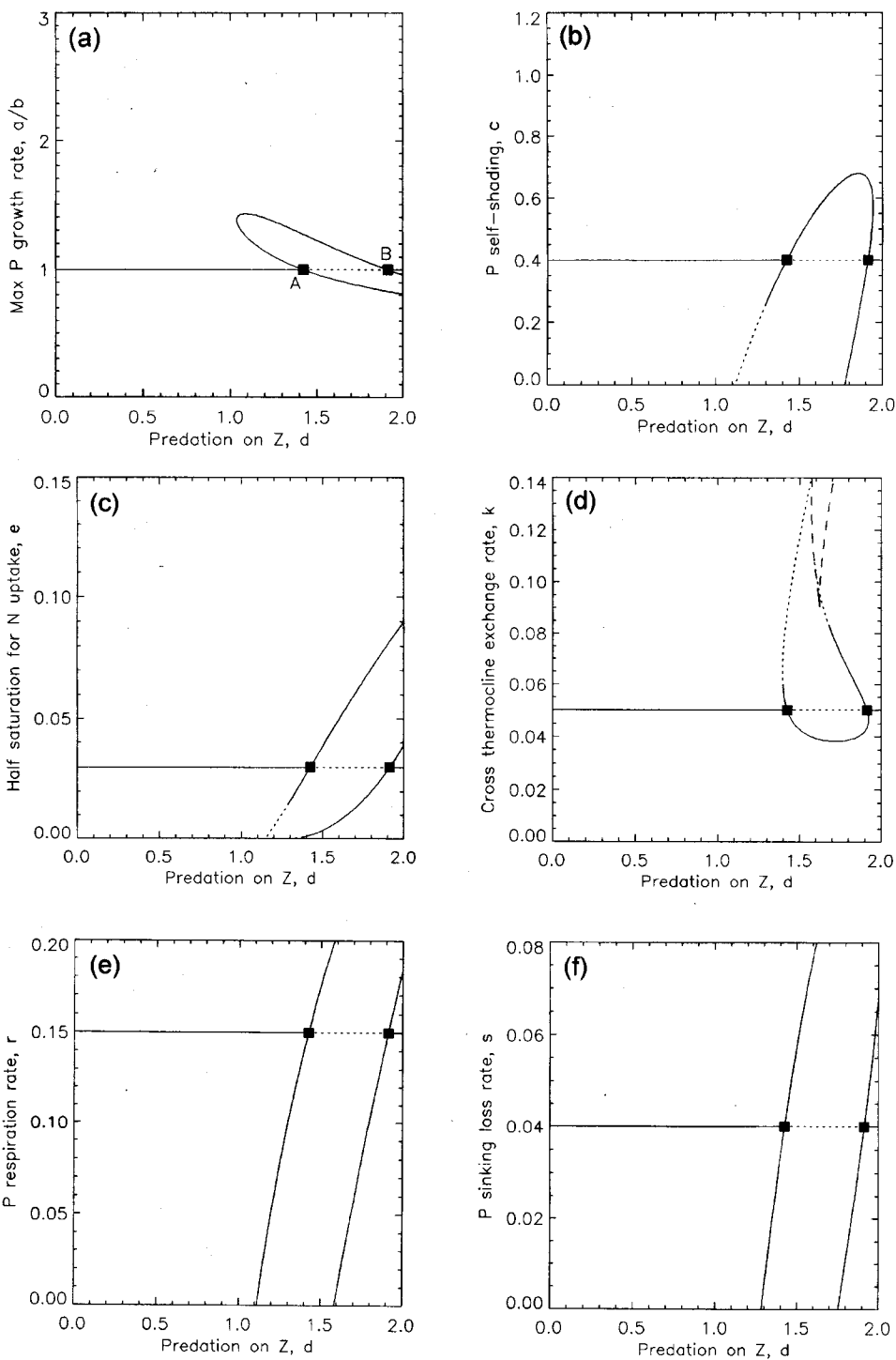


Fig. 4. Two-parameter bifurcation diagrams showing how the positions of the Hopf bifurcations in Fig. 3 change as each other parameter, together with d , is independently varied from its default value. In each case, Fig. 3 is shown as a horizontal line at the default parameter value, with the same key as for Fig. 3. The second parameter being varied in each figure is: (a) a/b ; (b) c ; (c) e ; (d) k ; (e) r ; (f) s ; (g) N_0 ; (h) α ; (i) β ; (j) γ ; (k) λ ; (l) μ . Hopf A and Hopf B are indicated in (a).

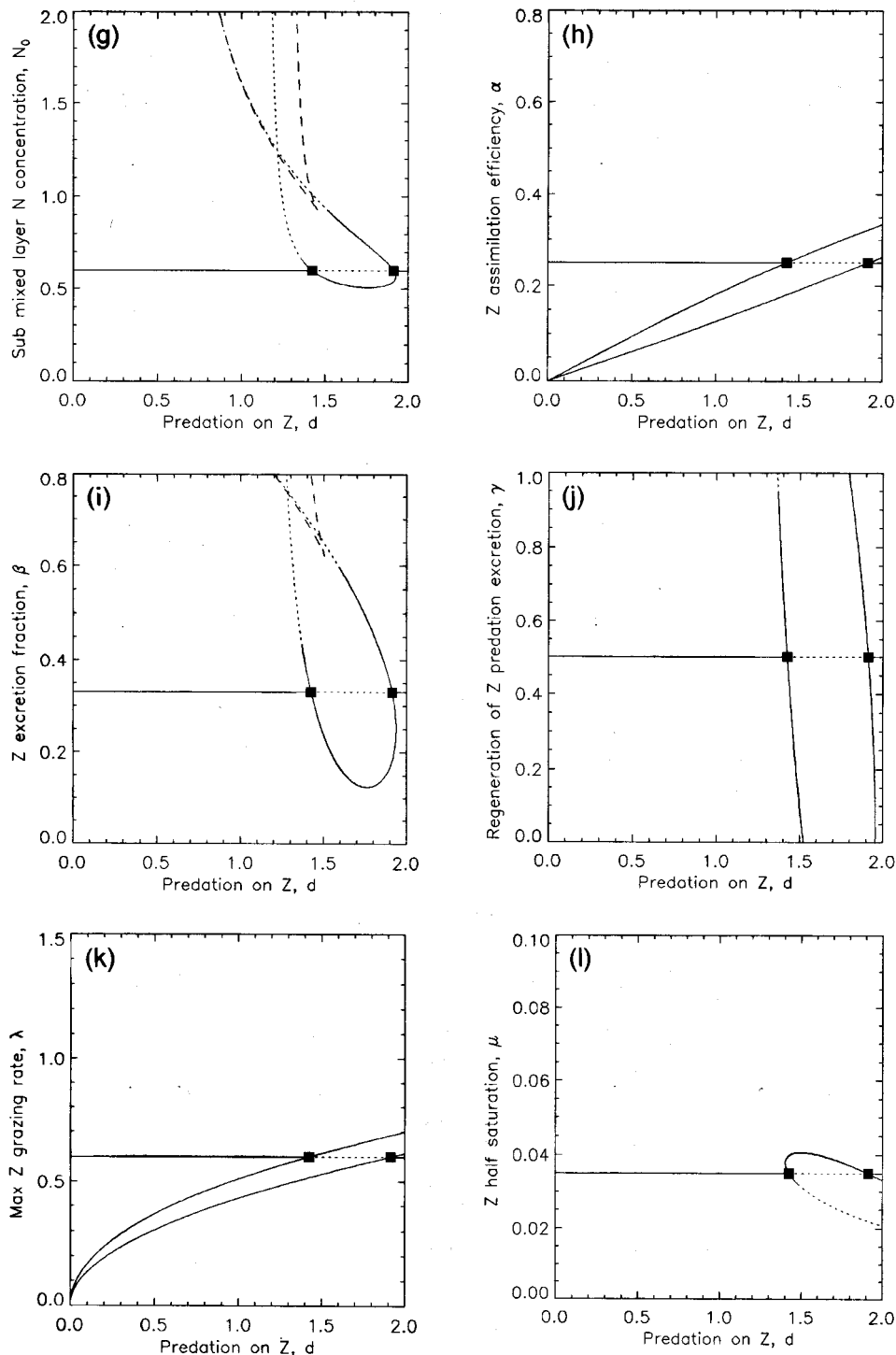


Fig. 4. (Cont.) The position of the supercritical Hopf bifurcations as each parameter is varied is given by the (non-horizontal) solid curves starting from the original Hopf bifurcations (the squares); a curve of short dashes indicates that a Hopf has become subcritical. In (d), (g) and (i) a curve of long dashes illustrates the locations at which the steady state undergoes fold bifurcations.

For each parameter, the bifurcation diagram from Fig. 3 is shown as a horizontal line at the default value of the parameter, since the parameter was held constant in Fig. 3. A solid horizontal line represents a stable equilibrium, a dashed horizontal line is unstable, and squares represent the Hopf bifurcations, as for Fig. 3. In the region of d where the equilibrium is unstable, limit cycles occur, as was illustrated in Fig. 3. In Fig. 4 the positions of the two Hopf bifurcations are tracked as both d and one other parameter are varied. A (non-horizontal) solid line shows the location of a supercritical Hopf bifurcation, and where it becomes dashed indicates that the Hopf bifurcation has become subcritical (meaning that the branch of periodic orbits emanating from it will be unstable and will coexist with the stable steady state). The curve of long dashes in Figs 4(d), (g) and (i) represent a fold bifurcation of the steady state. The effects of variations in a and b have been combined as a/b in a single diagram for the maximum phytoplankton growth rate, so that there are 12 distinct bifurcation diagrams.

Figure 4(a) shows that an increase in a/b (which can be considered as an increase in a or a decrease in b) causes the two Hopf bifurcations A and B from Fig. 3 to remain supercritical, but to coalesce at $a/b = 1.43$. Above this value, the steady state remains stable for all values of d , and does not undergo a Hopf bifurcation. A decrease in a/b causes the Hopf bifurcations to increase their d values, and eventually move out of the range of d which we are considering.

Figure 4(b) is the diagram for c , the phytoplankton self-shading parameter, against d . It is seen that an increase in c causes the Hopf bifurcations to remain supercritical and coalesce, as occurred in Fig. 4(a). As c is decreased from the default value, Hopf A becomes subcritical (dashed line), but at a value which is below 0.3, the minimum reported value of c . Thus, across the reported range of c , as d is varied, the steady state can either undergo two supercritical Hopf bifurcations, which are joined by a branch of stable limit cycles as in Fig. 3, or it simply remains stable.

The diagram for e , the half-saturation constant for nutrient uptake, Fig. 4(c), is qualitatively similar to that for c , but the Hopf bifurcations coalesce at a high value of d which is outside of our range. Thus, increasing e from the default value causes the region of stable limit cycles in the original diagram, Fig. 3, to shift to the right and move out of our range of d , as occurred in Fig. 4(a), resulting in just a single stable steady state for high e .

Figure 4(d) for k , the cross thermocline exchange rate, shows that increasing k causes Hopf A, and then Hopf B, to become subcritical. Figure 5(a) shows how the branch of limit cycles can still join up the Hopf bifurcations when $k = 0.07$ (for which Hopf A has become subcritical while Hopf B has remained supercritical). We wish to demonstrate qualitative effects and so only the nutrient value is shown, and the d scale is chosen to illustrate the region in question. Figure 5(a) is thus to be interpreted in the same way as Fig. 3(a). Solid circles still represent the maximum and minimum nutrient values for stable limit cycles, and the open circles represent the values for unstable cycles. The four open circles in Fig. 5(a) indicate the minimum nutrient value of the unstable cycle at the corresponding values of d . The maximum values cannot be seen on the diagram due to the proximity of the maximum stable limit cycle values to the Hopf bifurcation.

The stable limit cycle branch emanating from the supercritical Hopf B persists as d is decreased, and then undergoes a fold bifurcation at $d = 1.394$, and the resulting unstable cycles join up to the subcritical Hopf A at $d = 1.397$. A fold bifurcation of a limit cycle is similar to a fold bifurcation of a steady state—two

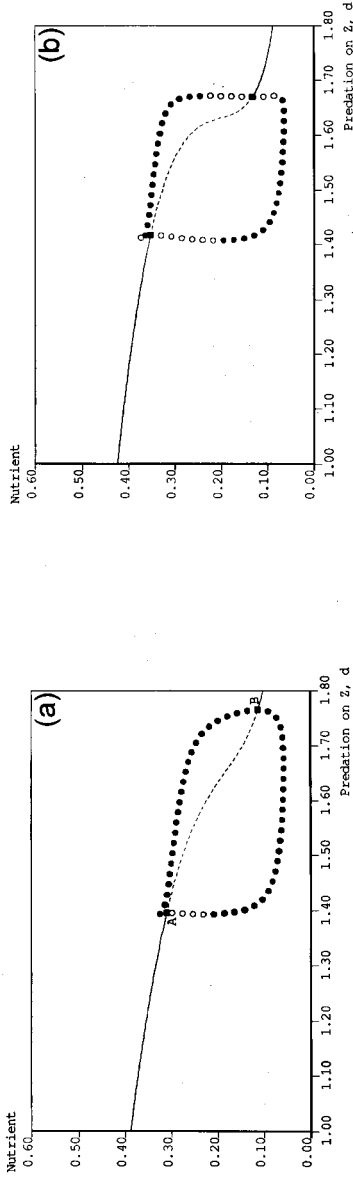


Fig. 5. The original Fig. 3(a) diagram of nutrient against d changes as k is increased. Open circles represent the maximum and minimum nutrient values for unstable cycles. (a) $k=0.07$ —Hopf A has become subcritical. The limit cycle branch undergoes a fold bifurcation and still joins up the two Hopf bifurcations. The open circles corresponding to the maximum nutrient values cannot actually be seen due to the close proximity of the fold bifurcation and Hopf bifurcation at $d \approx 1.40$. (b) $k=0.085$ —both Hopf bifurcations are subcritical and the limit cycle branch becomes stable via fold bifurcations close to each Hopf bifurcation.

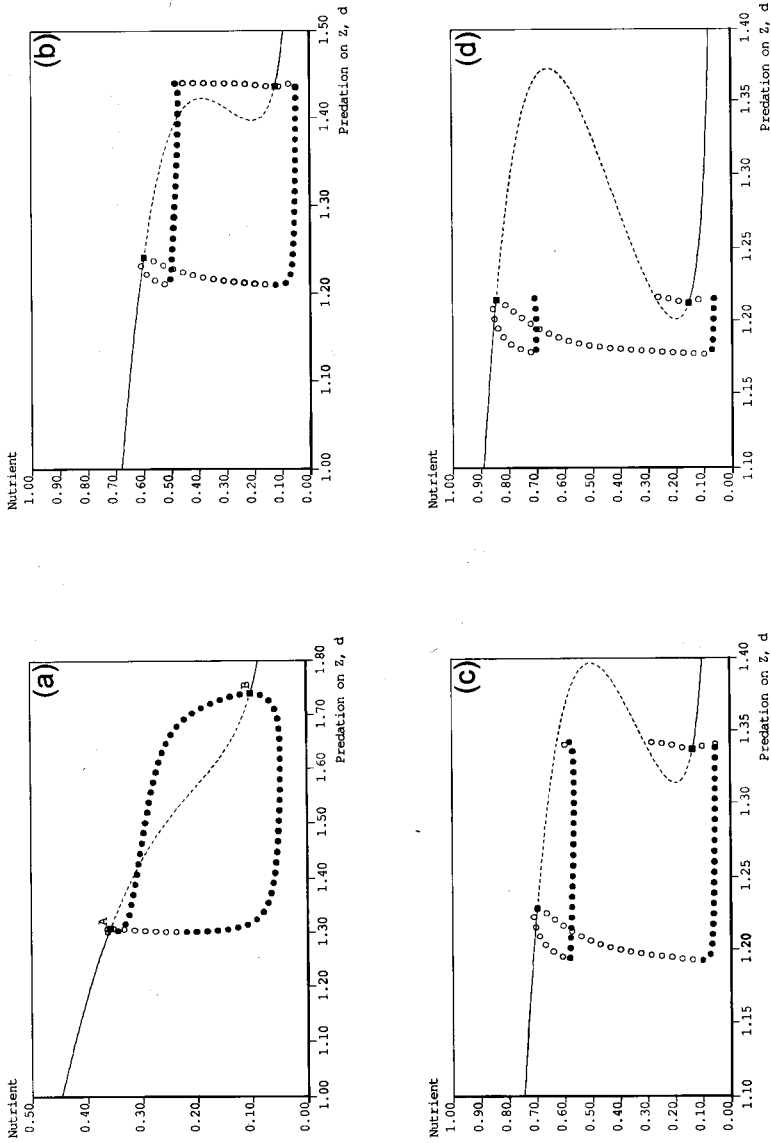


Fig. 6. The Fig. 3(a) diagram changes dramatically as N_0 is increased. (a) $N_0 = 0.75$ —Hopf A has become subcritical and the limit cycle branch is qualitatively the same as Fig. 5(a). (b) $N_0 = 1.0$ —a region of multiple unstable steady states exists, and a branch of limit cycles connects the two Hopf bifurcations. (c) $N_0 = 1.1$ —the unstable limit cycles near Hopf B now become homoclinic to the saddle point, and the Hopf bifurcations are no longer connected by a continuous branch of limit cycles.

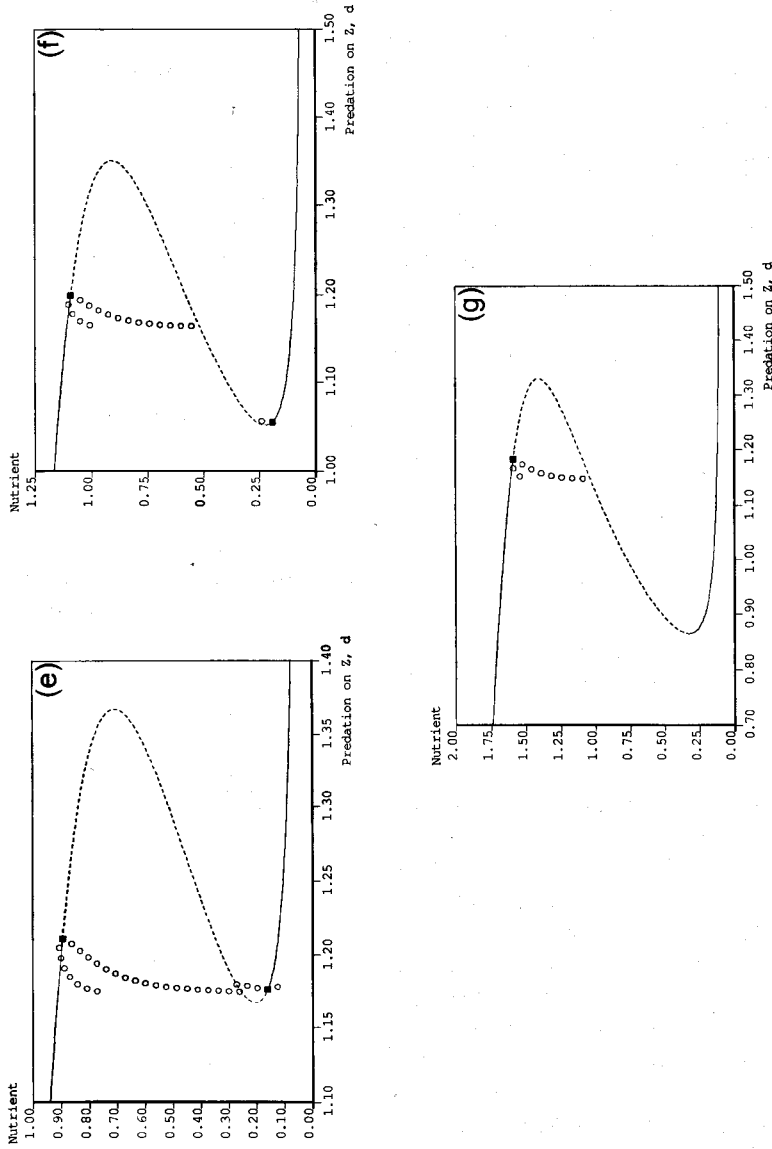


Fig. 6. (Cont.) (d) $N_0 = 1.25$ —the stable limit cycle branch now becomes homoclinic to the saddle point and the stable steady states exhibit hysteresis, and for $d \in (1.2123, 1.2145)$ the stable limit cycle coexists with two stable steady states. (e) $N_0 = 1.3$ —no fold bifurcations of the unstable limit cycle branch occur, thus no stable limit cycles arise and the unstable limit cycles become homoclinic, and the system exhibits hysteresis. (f) $N_0 = 1.5$ —similar to (e) except that the values of d at the homoclinic connections have crossed. (g) $N_0 = 2.0$ —Hopf A has now become a fold bifurcation.

cycles (of dissimilar stability) coexist for a particular parameter value, and as this parameter is decreased their orbits become closer together and then annihilate each other at the fold bifurcation; at values of the parameter below the fold bifurcation neither cycle exists. For clarity, fold bifurcations of limit cycles are not shown in Fig. 4. Thus, for the narrow region $d \in (1.394, 1.397)$ the stable steady state and stable limit cycle coexist, but for the remainder of the diagram the situation is qualitatively equivalent to Fig. 3(a), and in this case the fact that Hopf A has become subcritical as k has increased is fairly insignificant.

Figure 5(b) shows what happens when $k=0.085$ for which both Hopf bifurcations are now subcritical. The unstable branch from the subcritical Hopf B undergoes a fold bifurcation to become stable. This stable branch persists as d is decreased and undergoes another fold bifurcation to join up to Hopf A, in the same manner as for $k=0.07$. So, for $k=0.085$, there are two narrow regions of d for which a stable limit cycle and stable steady state coexist. For $k>0.091$, the steady state undergoes fold bifurcations (indicated by the curve of long dashes in Fig. 4(d)), and for $k>0.11$ only one Hopf bifurcation occurs; the consequent limit cycle behaviour shall be shown for an equivalent region in the N_0 diagram.

The diagrams for independent changes in phytoplankton respiration rate, r , phytoplankton sinking rate, s , and the regeneration of excretion by the predators on the zooplankton, γ , Figs 4(e), (f) and (j), respectively, are qualitatively very similar. Both Hopf bifurcations remain supercritical across the entire feasible ranges of each parameter and, furthermore, the length of the interval of d for which the limit cycle behaviour occurs remains virtually constant in each case. Thus, the model can be said to be insensitive to changes in these parameters, in the sense that varying each of them independently will cause hardly any change in the qualitative behaviour of the system. We note that r and γ represent recycling effects in the system (as is schematically shown in Fig. 1), but the model appears insensitive to the level (or absence) of such recycling. Furthermore, FDM90 found that their specific linear phytoplankton loss parameter (essentially $r+s$ in our model) was the most sensitive, and most difficult to determine, parameter in their system, whereas in our model such a loss is among the least sensitive parameters.

Figure 4(g) for the sub-mixed-layer nutrient concentration, N_0 , shows that increasing N_0 causes both Hopf bifurcations to become subcritical and then cross over (in terms of their d values). A curve of fold bifurcations of the steady state also arises (shown as a curve of long dashes). The qualitative changes in behaviour as N_0 is increased through this region are demonstrated in Fig. 6, and are discussed in Section 6. Qualitatively similar behaviour also occurs when β is varied, Fig. 4(i).

Figures 4(h) and (k) show that increasing α , the zooplankton assimilation efficiency, or λ , the maximum zooplankton grazing rate, causes the Hopf bifurcations to move out of the d range, as occurred for a decrease in a/b . Decreasing α or λ causes the Hopf bifurcations to be shifted towards $d=0$.

Finally, Fig. 4(l), for the zooplankton grazing half-saturation coefficient, μ , is similar to Fig. 4(a) for a/b , except that Hopf A becomes subcritical as μ is decreased, before it moves out of the range of d .

5.4 Bifurcation behaviour at different levels of N_0

The behaviour of the system as N_0 is increased is now discussed. At each fixed value of N_0 , the single bifurcation diagram of nutrient against d is shown in Fig. 6. Figure 6 thus indicates how the original bifurcation diagram in Fig. 3(a) changes

as we increase N_0 through Fig. 4(g); each Fig. 6 picture can therefore be considered as a horizontal slice through Fig. 4(g). Figure 4(g) only gives information about the bifurcations of the steady states; in Fig. 6, we also demonstrate the qualitative changes in limit cycle behaviour as N_0 is increased. Such changes can affect both the transient and asymptotic behaviour of the system. The scales of the Fig. 6 diagrams are not all the same, since they are chosen in order to highlight the qualitative changes that occur as N_0 is increased.

Figure 6(a), for $N_0=0.75$, shows essentially the same behaviour as Fig. 5(a) for $k=0.07$, whereby Hopf A is subcritical and Hopf B is supercritical, and the limit cycle branch undergoes a fold bifurcation close to Hopf A. Figure 6(b), for $N_0=1.0$, shows that the limit cycle branch joins up the two Hopf bifurcations in the same way as in Fig. 5(b) for $k=0.085$, but the unstable steady-state branch now undergoes two fold bifurcations; however, it does not regain stability in between the two Hopf bifurcations, and hence no new attractors appear. On Fig. 4(g), Hopf B becomes subcritical at $N_0=0.92$ and the fold bifurcations of the steady state appear (at a cusp point) at $N_0=0.93$; since these values are so close, we do not show the intermediate one-parameter bifurcation diagram in Fig. 6 (i.e. that for which Hopf B is subcritical and the steady state does not undergo a fold bifurcation).

Figure 6(c), for $N_0=1.1$, shows that the limit cycles now no longer form a single branch connecting up the two Hopf bifurcations. A region of stable limit cycles arises from Hopf A in the same manner as for $N_0=1.0$. This branch again undergoes a fold bifurcation (as d increases), but the resulting unstable branch then becomes homoclinic (as d then decreases) to the saddle point, rather than joining up to Hopf B. In other words, the cycle in N - P - Z space approaches the saddle point, leading ultimately to a homoclinic connection in which the unstable manifold of the saddle point joins up in a loop (formerly the cycle) with its own stable manifold; see Thompson and Stewart (1986) or Wiggins (1990) for further details.

The unstable branch which arises from Hopf B also terminates at a homoclinic connection to the saddle point (at a different d value). The behaviour of the stable attractors has not qualitatively changed from $N_0=1.0$, but as N_0 is increased further it is the stable limit cycle branch which becomes homoclinic to the saddle point, as illustrated in Fig. 6(d) for $N_0=1.25$.

Hopf A now occurs at a slightly higher value of d than Hopf B, as illustrated by the crossing of the Hopf bifurcation curves at $N_0=1.24$ in Fig. 4(g). For $N_0=1.25$, Fig. 6(d), the system therefore exhibits hysteresis behaviour (whereby two stable steady states coexist at the same value of d). The stable limit cycle branch still exists, and coexists with at least one of the stable steady states; for the (rather pathological) narrow region $d \in (1.2123, 1.2145)$ there are three coexisting stable attractors, namely two stable steady states plus a stable limit cycle. As d increases from this region, one steady state becomes unstable at the Hopf A, and then the stable limit cycle branch disappears at a homoclinic connection (or a blue sky catastrophe—it disappears 'into the blue' (Thompson & Stewart, 1986)), and the lowest steady-state branch becomes the sole attractor.

At $N_0=1.3$, Fig. 6(e), the fold bifurcation of the unstable limit cycle branch from Hopf A no longer occurs and this branch does not become stable; instead it becomes homoclinic to a saddle point (as does the branch from Hopf B) and no stable limit cycles exist. The system undergoes hysteresis, indicated by the region of coexisting stable steady states. Figure 6(f), for $N_0=1.5$, shows how the

homoclinic connections of the unstable limit cycle branches have shifted along the saddle point branch. Figure 6(g), for $N_0 = 2.0$, shows that Hopf B has disappeared and the steady state loses stability due to a fold bifurcation (the Hopf bifurcation curve in Fig. 4(g) terminates at $N_0 = 1.97$ when it joins up with the fold curve).

6 Discussion

The primary aim of this paper has been to explore and display the qualitative behaviour of a simple NPZ model across a whole range of parameter values used in the literature on plankton population dynamics. To a certain extent, this range reflects the different physical conditions in specific geographical locations, but to a greater extent it reflects uncertainties in the actual values to be ascribed to the parameters. Both these reasons strongly motivate thorough investigation of theoretical models.

Thus, we have systematically built up a comprehensive, but by no means complete, picture of the bifurcation behaviour of the system. We started with the parameters set at their default values, and showed that qualitatively different behaviour of the trajectories occurred at two distinct values of d , measuring the higher predation on zooplankton. This difference was illustrated in Fig. 3, which showed how the steady-state values and limit cycle amplitudes of the nutrient, phytoplankton and zooplankton concentrations changed as d was varied; somewhat surprisingly, the zooplankton concentrations showed the least variation, even though it was the higher predation on them which was being altered. The period of the oscillations was 35 days, in agreement with the oscillatory behaviour discussed by Ryabchenko *et al.* (1996). This period was insensitive to the value of d , implying that the fundamental frequency of the oscillations is controlled by some other specification of the system; this is the focus of current work.

Figure 4 then demonstrated how this picture can qualitatively change as a second parameter is varied, and showed that changing some of the parameters caused the oscillatory region to disappear. The parameters which, when varied, demonstrated persistence of the oscillatory behaviour across a similar range of d as in Fig. 3, were r , s and γ . As discussed, the model may have been expected to show greater sensitivity to such parameters. We then showed how the original one-parameter bifurcation diagrams change significantly as the sub-mixed-layer nutrient level, N_0 , is increased, displaying a rich array of bifurcation behaviour, including destruction of limit cycles at homoclinic connections.

The broad picture which emerges is that parameter space is divided into large regions where either a single stable equilibrium or a single attracting limit cycle exists, implying oscillatory behaviour. There are also small, but possibly important regions where the dynamics is more complex, with multiple attractors, so that, for example, two stable equilibria, or a stable equilibrium and a stable limit cycle coexist.

Although, as is usual in bifurcational analysis, we have dwelt on the character of the asymptotic attractors (for large time) of the system, it is important to note that transient behaviour of trajectories is much affected, even for far shorter times, by that character. However, the trajectories which we have shown, in common with further simulations using other initial conditions and parameter values, indicate that the attractors are actually reached after a relatively short transient time.

Oscillatory behaviour is seen here to be widely possible, raising further important questions about the response of plankton populations to periodic (seasonal) forcing (see Ryabchenko *et al.*, 1996). Such forcing may push a system into and out of an

oscillatory phase during the course of a year. Moreover, the details of the oscillations, and indeed of the transient approaches to stable equilibria, can and do show wide variations even within the regions of stable persistence of the actual attractors. These details are of course likely to be of importance in the biological context and will be reported elsewhere.

Acknowledgements

AME acknowledges the support of the William Wright Smith Scholarship from the University of Leeds. We thank Carsten Knudsen and David Knapp for assistance with this work, and John Steele for several helpful suggestions.

References

- Adams, J. A. and Steele, J. H. (1966) Shipboard experiments on the feeding of *Calanus finmarchicus* (Gunnerus). *Some Contemporary Studies in Marine Science* (ed. H. Barnes; George Allen & Unwin, London), pp. 19–35.
- Armstrong, R. A. (1994) Grazing limitation and nutrient limitation in marine ecosystems: steady state solutions of an ecosystem model with multiple food chains. *Limnology and Oceanography* **39**, 597–608.
- Doedel, E., Wang, X. and Fairgrieve, T. (1990) AUTO: software for continuation and bifurcation problems in ordinary differential equations. Applied Mathematics Report, California Institute of Technology, CA.
- Evans, G. T. and Parslow, J. S. (1985) A model of annual plankton cycles. *Biological Oceanography* **3**, 327–347.
- Fasham, M. J. R. (1993) Modelling the marine biota. *The Global Carbon Cycle* (ed. M. Heimann; Springer, Berlin), pp. 457–504.
- Fasham, M. J. R. (1995) Variations in the seasonal cycle of biological production in subarctic oceans: a model sensitivity analysis. *Deep-Sea Research I* **42**, 1111–1149.
- Fasham, M. J. R., Ducklow, H. W. and McKelvie, S. M. (1990) A nitrogen-based model of plankton dynamics in the oceanic mixed layer. *Journal of Marine Research* **48**, 591–639.
- Fasham, M. J. R., Sarmiento, J. L., Slater, R. D., Ducklow, H. W. and Williams, R. (1993) Ecosystem behavior at Bermuda Station “S” and Ocean Weather Station “India”: a general circulation model and observational analysis. *Global Biogeochemical Cycles* **7**, 379–415.
- Franks, P. J. S., Wroblewski, J. S. and Flierl, G. R. (1986) Behavior of a simple plankton model with food-level acclimation by herbivores. *Marine Biology* **91**, 121–129.
- Frost, B. W. (1987) Grazing control of phytoplankton stock in the open subarctic Pacific Ocean: a model assessing the role of mesozooplankton, particularly the large calanoid copepods *Neocalanus* spp. *Marine Ecology Progress Series* **39**, 49–68.
- Guckenheimer, J., Myers, M. R., Wicklin, F. J. and Worfolk, P. A. (1991) Dstool: a dynamical system toolkit with an interactive graphical interface. Center for Applied Mathematics, Cornell University, New York.
- Hastings, A. and Powell, T. (1991) Chaos in a three-species food chain. *Ecology* **72**, 896–903.
- Henderson, E. W. and Steele, J. H. (1995) Comparing models and observations of shelf plankton. *Journal of Plankton Research* **17**, 1679–1692.
- Hofmann, E. E. and Ambler, J. W. (1988) Plankton dynamics on the outer southeastern U.S. continental shelf. Part II: a time dependent biological model. *Journal of Marine Research* **46**, 883–917.
- Khibnik, A. I., Kuznetsov, Y. A., Levitin, V. V. and Nikolaev, E. V. (1992) *Interactive LOCAL BIFurcation analyzer* (Computer Algebra, Netherlands).
- Levitin, V. and Khibnik, A. (1991) *TraX simulation and analysis of dynamical systems* (Applied Biomathematics, New York).
- McCann, K. and Yodzis, P. (1995) Bifurcation structure of a three-species food chain model. *Theoretical Population Biology* **48**, 93–125.
- Parsons, T. R., LeBrasseur, R. J., Fulton, J. D. and Kennedy, O. D. (1969) Production studies in the Strait of Georgia. Part II. Secondary production under the Fraser River plume, February to May, 1967. *Journal of Experimental Marine Biology and Ecology* **3**, 39–50.
- Ryabchenko, V. A., Fasham, M. J. R., Kagan, B. A. and Popova, E. E. (1996) What causes short-term oscillations in ecosystem models of the ocean mixed layer? *Journal of Marine Systems* (in press).

- Sarmiento, J. L., Slater, R. D., Fasham, M. J. R., Ducklow, H. W., Toggweiler, J. R. and Evans, G. T. (1993) A seasonal three-dimensional ecosystem model of nitrogen cycling in the North Atlantic euphotic zone. *Global Biogeochemical Cycles* 7, 417–450.
- Steele, J. H. and Frost, B. W. (1977) The structure of plankton communities. *Philosophical Transactions of the Royal Society of London, Series B* 280, 485–534.
- Steele, J. H. and Henderson, E. W. (1981) A simple plankton model. *American Naturalist* 117, 676–691.
- Steele, J. H. and Henderson, E. W. (1992) The role of predation in plankton models. *Journal of Plankton Research* 14, 157–172.
- Steele, J. H. and Henderson, E. W. (1993) The significance of interannual variability. *Towards a Model of Ocean Biogeochemical Processes* (eds G. T. Evans and M. J. R. Fasham; Springer, Berlin), pp. 237–260.
- Taylor, A. H. and Joint, I. (1990) A steady-state analysis of the 'microbial loop' in stratified systems. *Marine Ecology Progress Series* 59, 1–17.
- Thompson, J. M. T. and Stewart, H. B. (1986) *Nonlinear Dynamics and Chaos* (John Wiley, Chichester).
- Truscott, J. E. (1994) Temporal and spatial behaviour of plankton ecosystems. PhD thesis, University of Leeds.
- Truscott, J. E. and Brindley, J. (1994) Equilibria, stability and excitability in a general class of plankton population models. *Philosophical Transactions of the Royal Society of London, Series A* 347, 703–718.
- Wiggins, S. (1990) *Introduction to Applied Nonlinear Dynamical Systems and Chaos* (Texts in Applied Mathematics, Vol. 2; Springer, New York).
- Williams, R. (1988) Spatial heterogeneity and niche differentiation in oceanic zooplankton. *Biology of Copepods. Hydrobiologia* (eds G. A. Boxshall and H. K. Schimke) 167/168, 151–159.
- Wroblewski, J. S. (1989) A model of the spring bloom in the North Atlantic and its impact on ocean optics. *Limnology and Oceanography* 34, 1563–1571.